Solar Energy Materials & Solar Cells 121 (2014) 176–181

Contents lists available at ScienceDirect

Solar Energy Materials & Solar Cells

journal homepage: www.elsevier.com/locate/solmat

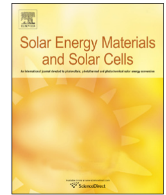

# Effects of indium concentration on the efficiency of amorphous In–Zn–O/$SiO_x$/$n$-Si hetero-junction solar cells

Hau-Wei Fang [a], Tsung-Eong Hsieh [a,*], Jenh-Yih Juang [b]

[a] Department of Materials Science and Engineering, National Chiao Tung University, 1001 Ta-Hsueh Road, Hsinchu 30010, Taiwan, ROC
[b] Department of Electrophysics, National Chiao Tung University, 1001 Ta-Hsueh Road, Hsinchu 30010, Taiwan, ROC

ARTICLE INFO

*Article history:*
Received 22 May 2013
Received in revised form
31 October 2013
Accepted 1 November 2013
Available online 30 November 2013

*Keywords:*
Indium zinc oxide
Pulsed laser deposition
Hetero-junction structure solar cells

ABSTRACT

Semiconductor–insulator–semiconductor (SIS) hetero-junction solar cells comprising of the amorphous indium zinc oxide ($a$-IZO) layer directly deposited onto the n-type Si substrates by pulsed laser deposition were fabricated. Characterizations on the physical properties of the $a$-IZO layer and the $a$-IZO/$SiO_x$ interface as a function of In/(Zn+In) ratio were carried out to delineate their influences on the photovoltaic performance of SIS solar cells. The optical and electrical analyses indicated that the resistivity of $a$-IZO films decreased with increasing In concentration, reaching $4.5\times10^{-4}$ Ω-cm for In/(Zn+In)=0.5, which also exhibited a transmittance higher than 80% in the visible-light wavelength range. Moreover, combining with an optimally controlled insulating $SiO_x$ layer (about 2.0 nm), the device exhibited excellent SIS solar cell performance with open-circuit voltage of 0.38 V, short-circuit current density of 45.1 mA cm$^{-2}$, fill factor of 49.7% and a conversion efficiency of 8.4% under the AM1.5 illumination condition. The dramatic performance enhancement was attributed to the reduction of effective interface trap densities at the $a$-IZO/$SiO_x$ interface and the increase of carrier mobility in the $a$-IZO layer resulted from the increase of In/(In+Zn) ratio.

© 2013 Elsevier B.V. All rights reserved.

## 1. Introduction

The photovoltaic devices based on transparent conducting oxides (TCOs) such as semiconductor–insulator–semiconductor (SIS) heterojunction solar cells have attracted extensive research interests due to the advantages of relatively high conversion efficiency ($\eta$), simple device structure, easy manufacturing process and low production cost. Various TCOs, *e.g.*, indium tin oxide (ITO) [1–3], tin oxide ($SnO_2$) [4] and zinc oxide (ZnO) [5] have been deposited on silicon (Si) wafer substrates clad with a thin $SiO_x$ layer to form the SIS devices and the $\eta$ values in those reports were 10%, 7.8% and 6.9%, respectively. However, in abovementioned studies, the TCOs were all deposited at relatively high temperatures (>400 °C) to yield the required polycrystalline structure. This is adverse to the thermal budget of manufacturing process.

Recently, amorphous TCOs such as amorphous indium zinc oxide ($a$-IZO) films have received tremendous attention because of their wide optical bandgap ($E_g$>3.3 eV), high carrier mobility (>10 cm$^2$ V$^{-1}$ s$^{-1}$) and high carrier concentration (>10$^{20}$ cm$^{-3}$) properties, which are suitable for the optoelectronic applications. In particular, the relatively low In content and deposition temperature have made $a$-IZO a promising alternative for the fabrication of SIS solar cells in comparison with ITO. In the TCO/$SiO_x$/Si SIS solar cells, it has been pointed out that the thickness of the $SiO_x$ layer and the presence of interface states are the key factors affecting the SIS device performance [1]. In general, the thickness of the $SiO_x$ layer has to be limited to about 2 nm in order to efficiently separate the TCO layer and Si substrate and serve as the tunneling layer of electrons from Si substrate to the TCO layer. In our previous studies of $a$-IZO/$SiO_x$/Si SIS solar cells [6,7], various growth methods of $SiO_x$ layers including the wet process (immersing the Si substrate in a hot $H_2O_2$ solution to form the $SiO_x$ layer) and the dry thermal oxidization (forming the $SiO_x$ layer by *in-situ* heating the Si substrate in vacuum chamber prior to the $a$-IZO deposition) were performed. It was found that indeed the quality of $SiO_x$ layer plays a critical role in the SIS solar cell performance. For instance, the dry method was found to result in denser $SiO_x$ layer with lower interface trap densities ($D_{it}$) at the $a$-IZO/$SiO_x$ and $SiO_x$/Si interfaces, which in turn leads to over 50% improvement in the $\eta$ value of the SIS devices from 2.2% [6] to 3.4% [7]. The above results also suggest that $\eta$ may be further improved if the effective $D_{it}$ at the $SiO_x$/Si and $a$-IZO/$SiO_x$ interfaces can be reduced by pre-occupied part of the interface states with free carriers, such that more photo-excited electrons can be harvested. In practice, the thickness of $SiO_x$ layer and $D_{it}$ at the $SiO_x$/Si interface are determined by the condition of the dry thermal oxidization and can be regarded as a fixed parameter. On the other hand, it might be possible to manipulate the effective $D_{it}$ at $a$-IZO/$SiO_x$ interface by changing the carrier density in the $a$-IZO layer.

* Corresponding author. Tel.: +886 3 5712121x55306; fax: +886 3 5724727.
*E-mail address:* tehsieh@mail.nctu.edu.tw (T.-E. Hsieh).

0927-0248/$ - see front matter © 2013 Elsevier B.V. All rights reserved.
http://dx.doi.org/10.1016/j.solmat.2013.11.003

In this work, we investigate the effects of carrier concentration in the *a*-IZO layer on the photoelectric characteristics of a series of *a*-IZO/$SiO_x$/Si SIS devices by varying the In/(Zn+In) ratio while keeping the $SiO_x$/Si parts identical. Systematic examinations on the microstructures, electrical, optical properties were carried out on the *a*-IZO films. In particular, the photo-responsive capacitance–voltage (*C*–*V*) measurement [8,9] was performed to evaluate the $D_{it}$ property at *a*-IZO/$SiO_x$ interface and its influences on the SIS solar cell performance are discussed as follows.

## 2. Experimental

The *a*-IZO films were separately deposited on Corning 1737 glass plates and n-type Si(1 0 0) wafers (resistivity=2–5 Ω-cm) by pulsed laser deposition (PLD). The mixtures of $In_2O_3$ and ZnO powders (supplier: Gredmann; purity: 99.999%) with In/(Zn+In) ratios of 0.25, 0.4 and 0.5 were used for preparing the PLD targets. In order to obtain the compact pellets, the $In_2O_3$–ZnO powder mixtures were homogenized by attrition milling, pre-calcined at 600 °C for 6 h in air, and then pressed at 10 psi in disc form with a diameter of 1 in. Finally, the pellets were sintered at 1250 °C for 2 h to form the PLD targets.

Before being transferred into the vacuum chamber, the glass substrates were cleaned sequentially in de-ionized water, acetone and ethanol (10 min for each step). The Si wafers were cleaned with a buffered oxide etching solution comprised of 40% $NH_4F$ and 49% HF in a volume ratio of 6:1 for 3 min to remove the native oxide layer. The KrF excimer laser (Compex 201, $\lambda$=248 nm) was used to ablate the PLD target with an energy density of 3.8 J $cm^{-2}$ per pulse and a repetition rate of 5 Hz. The background pressure of the PLD vacuum chamber was $4.0\times10^{-6}$ Torr. The distance between the target and the substrate was kept at 4 to 5 cm and the substrate temperature was kept at 250 °C during the deposition. In order to obtain the low-resistivity *a*-IZO films, high-purity argon (Ar; 99.999%) with a flow rate of 6.0 sccm was introduced into the chamber and the working pressure was maintained at 4.2 m Torr. The thickness of *a*-IZO films determined by the ellipsometry (SOPRA, GES-5) and alpha-step profilometer (KOSAKA, ET300) was in the range of 25 to 35 nm. Afterward, 100-nm thick aluminum (Al) metal layers were deposited by *e*-beam evaporation to form the bottom electrodes on the backside of Si substrates and the top finger electrodes on *a*-IZO layers, respectively.

The crystallinity of *a*-IZO films was examined by X-ray diffraction (XRD; REGAKU) with $\lambda_{Cu-K\alpha}$ of 0.15405 nm and a transmission electron microscope (TEM; JEOL JEM-2100F) operated at 200 kV. The transport properties of *a*-IZO films were determined by the Hall measurement (ECOPIA HMS-3000) in a constant magnetic field of 0.58 T. The optical transmittance of *a*-IZO films was measured in the wavelength range of 300 to 1600 nm by an UV–vis–NIR spectrometer (JASCO V-650). The $D_{it}$ values were deduced from the photo-responsive *C*–*V* measurements equipped with a 20-W halogen lamp as the light source and a Wayne Kerr 6520B precision LCR meter operating at the frequency of 100 kHz. In order to differentiate the influence of bulk defects in *a*-IZO layer from that of interfacial defects at *a*-IZO/$SiO_x$ interface, the *C*–*V* characteristics of Al/*a*-IZO/Al and Al/*a*-IZO/$SiO_x$ samples were also analyzed by using a Wayne Kerr 6520B precision LCR meter at 100 kHz. The performance of the *a*-IZO/$SiO_x$/*n*-Si SIS solar cells were measured in a solar cell efficiency measurement system equipped with a xenon lamp and a Keithley 2400 *I*–*V* source meter under the AM1.5 illumination condition. The incident photon-to-current conversion efficiency (IPCE) was measured with a xenon lamp and a Keithley 2400 source meter in the wavelength range of 400 to 1400 nm.

## 3. Results and discussion

Fig. 1 presents the XRD profiles of *a*-IZO films deposited on glass substrates at 250 °C using the IZO targets with various In/(Zn+In) ratios. It is evident that, in the detected diffraction angle (2$\theta$) ranging from 20 to 60°, no characteristic peak can be identified except for a broad low-intensity peak occurring in the range of 2$\theta$=30 to 35°, indicating that the IZO films are amorphous or of the nano-crystalline structure [10,11]. Moreover, the broad XRD peak shifts toward lower diffraction angles with the increase of In content. It is noted that 2$\theta$ of 30.6° and 34.4° can be assigned to the diffraction peaks of $(2\,2\,2)_{In_2O_3}$ and $(0\,0\,2)_{ZnO}$, respectively. The peak shift might thus be ascribed to the $In^{3+}$ ($r$~0.080 nm) substitution for the $Zn^{2+}$ ($r$~0.074 nm) in IZO lattice, which is expected to result in a lattice expansion. Using the targets with different In contents to prepare IZO films, Minami et al. [12] and Naghavi et al. [13] also reported a similar lower-angle-shift of XRD peak with the increase of In content.

Fig. 2 summaries the transport properties of *a*-IZO films obtained by the Hall measurement. The resistivity of *a*-IZO film decreases with the increase of In/(Zn+In) ratio and the sample with In/(Zn+In) of 0.5 exhibits the lowest resistivity of $4.5\times10^{-4}$ Ω-cm. All *a*-IZO films exhibit n-type conducting behaviors and the carrier concentration increases from $2.0\times10^{20}$ to $8.5\times10^{20}$ $cm^{-3}$ when the In/(Zn+In) ratio increases from 0.25 to 0.5, indicating that the resistivity decrement is correlated to the increase of carrier concentration. The enhancement of n-type carrier concentration is a natural consequence of doping higher valence $In^{3+}$ into ZnO [14]. Moreover, it is also evident that the increase of In/(Zn+In) ratio results in a moderate increase of Hall mobility from 12 to 16 $cm^2\,V^{-1}\,s^{-1}$. Previous studies [15,16] reported that the Hall mobility of *a*-TCOs comprising $(n-1)d^{10}ns^0$ ($n\geq4$) cation dopants are insensitive to the structural

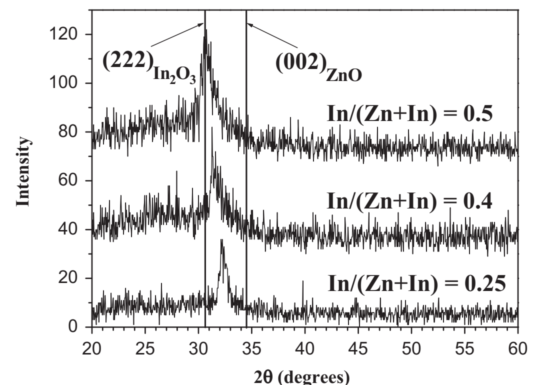


**Fig. 1.** XRD profiles of *a*-IZO films prepared on glass substrates using the IZO targets with different In/(Zn+In) ratios.

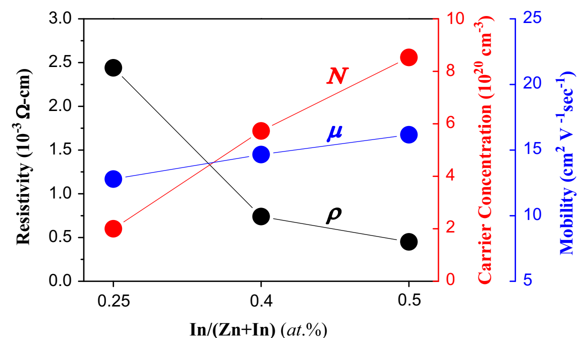


**Fig. 2.** Resistivity ($\rho$), carrier concentration ($N$), and mobility ($\mu$) of *a*-IZO films prepared on glass substrates using the IZO targets with different In/(Zn+In) ratios.

disorder because of the large overlap between the *ns* orbitals. Thus, the improved Hall mobility observed in the present *a*-IZO films can be attributed to more abundant percolated conduction paths arising from the overlapping of In 5s orbitals.

Optical transmittances of the *a*-IZO films with various In/(Zn+In) ratios are presented in Fig. 3. The average transmittances exceed 80% in the visible-light to NIR wavelength region for all *a*-IZO films, indicating that In content has negligible effects on the film transmittance. However, the absorption edge appears to shift toward the short wavelength side with the increase of In content. This can be explained by the Burstein–Moss effect [17] induced by the increase of the carrier concentration in the *a*-IZO film. Alternatively, it might be due to the blunted curvature of conduction band resulted from the amorphous structure [18]. For a direct bandgap semiconductor [19], the $E_g$ of sample can be obtained from the Tauc plot [20], *i.e.*, the plot of $(\alpha h\nu)^r$ against $h\nu$, where $\alpha$ is the absorption coefficient, $h$ is Plank's constant, $\nu$ is the frequency of the incident photon and $r=2$ for amorphous oxide semiconductors, respectively [19]. As shown in the inset of Fig. 3, the $E_g$ of *a*-IZO films increases from 3.37 to 3.54 eV when the In/(Zn+In) ratio increases from 0.25 to 0.5.

Fig. 4 shows the cross-sectional TEM image of the SIS device containing *a*-IZO film with In/(Zn+In)=0.5. An ultra-thin $SiO_x$ layer with the thickness about 2.03 nm can be seen at the interface between the Si substrate and *a*-IZO layer. In addition to the microstructure and properties of *a*-IZO layers, the geometry of $SiO_x$ layer is known to affect the tunneling current and, hence, is correlated to the SIS device performance [6,21]. The thickness of $SiO_x$ layer in our SIS sample is in agreement with the optimum thickness of about 2 nm obtained from our previous studies on the Si-based SIS solar cells [7]. Thus, the SIS device characteristics presented in the following should be able to delineate the effects arising from the properties of the top *a*-IZO layer. Moreover, the distribution of lattice fringes in *a*-IZO region (see Fig. 4) reveals that the *a*-IZO layer is in nano-crystalline form with grain size of a few nanometers. This is in agreement with the XRD results presented in Fig. 1, indicating that the *a*-IZO layers deposited on both the Si and glass substrates are of the same microstructure.

The current density-applied voltage (*J–V*) characteristics of the SIS devices measured in dark environment at room temperature are shown in Fig. 5. The results depict a rectifying characteristic with a turn-on voltage at a forward bias (positive bias on *a*-IZO) of about 0.48 V for all samples. To explain this, we schematically plot the corresponding band diagram of the SIS device in Fig. 6. In this plot, $\phi_{I-S}$ of 4.6 eV and $\phi_{S-I}$ of 4.1 eV are the electron affinities for *a*-IZO and Si, respectively. According to Ponpon et al. [22], the difference between $\phi_{S-I}$ and $\phi_{I-S}$ gives the theoretical upper limit of the barrier height, $\phi_B \approx 0.5$ eV, in good agreement with forward turn-on bias of 0.48 V seen in Fig. 5. Consequently, the interfacial $SiO_x$ layer at the *a*-IZO/Si interface might serve as a double Schottky barrier between both n-type layers. Under the forward bias, the band bending at Si/$SiO_x$ interface will gradually induce an inversion region for SIS devices due to the presence of the built-in electric field. Moreover, the current is dominated by the electrons in *n*-Si tunneling through the $SiO_x$ layer into the *a*-IZO film due to the relatively large $\phi_{S-I}$. In such a case, the increase of the electron concentration arising from the In-doping in the *a*-IZO layers enhances the band bending at the *a*-IZO/$SiO_x$ interface. Giving that the structure is consisted of three layers and at least two pivotal oxide/semiconductor interfaces, the 10% variation of the

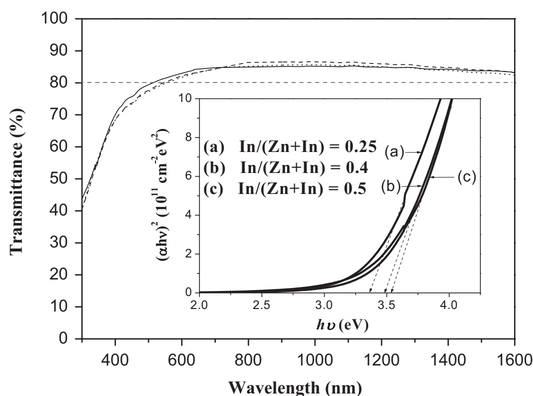


**Fig. 3.** Transmittance spectra of *a*-IZO films prepared at various In content ratios. The inset shows the determination of $E_g$ by extrapolating the Tauc plot of $(\alpha h\nu)^2$ against $h\nu$.

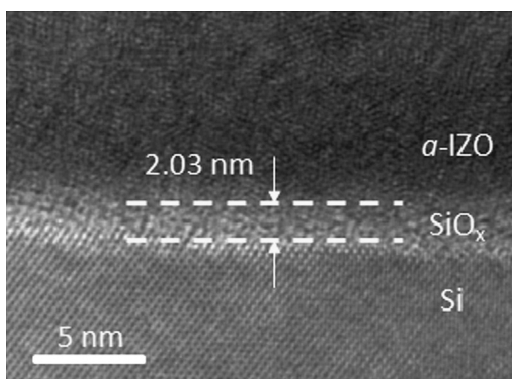


**Fig. 4.** Cross-sectional TEM micrographs of the SIS device with In/(Zn+In)=0.5.

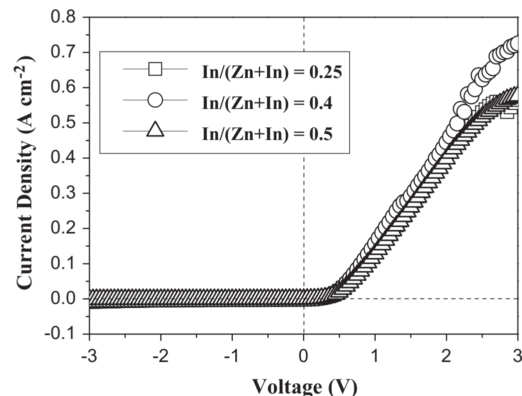


**Fig. 5.** *J–V* characteristic of *a*-IZO/$SiO_x$/*n*-Si devices measured in the dark condition.

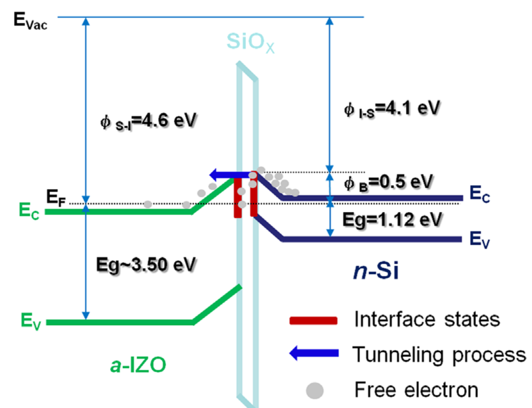


**Fig. 6.** Schematic energy band diagram of *a*-IZO/$SiO_x$/*n*-Si hetero-junction structure.

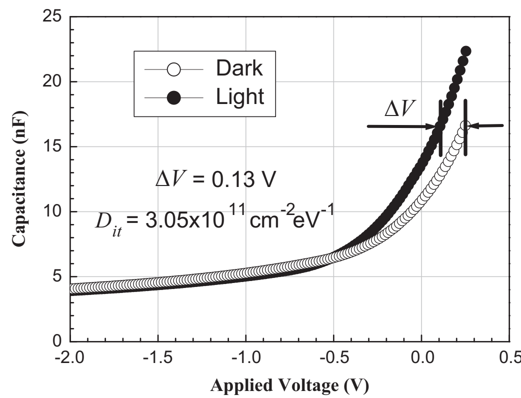


**Fig. 7.** Photoresponsive $C$–$V$ illustration for SIS devices prepared at In/(Zn+In)=0.25.

tunneling current density (namely in the range from 0.58 to 0.70 A $cm^{-2}$ observed in Fig. 5) is considered to be reasonable.

Theoretical studies by Shewchun et al. [1–3] indicated that the value of $\phi_B$ is intimately correlated with the open-circuit voltage ($V_{oc}$) of SIS devices. Consequently, the presence of interfacial states may affect the carrier tunneling process and suppress the $V_{oc}$ of SIS devices. In order to evaluate the properties at the $a$-IZO/$SiO_x$ and $SiO_x$/Si interfaces, photo-responsive $C$–$V$ measurements were performed and the magnitude of $D_{it}$ was estimated by the following equation [8,9]:

$$D_{it} = C_i \Delta V / qE_g \tag{1}$$

where $C_i$ is the insulator layer capacitance, $\Delta V$ is the voltage shift caused by the photo-induced change in charges at the $a$-IZO/$SiO_x$ and $SiO_x$/Si interfaces, and $q$ is the electron charge, respectively. As shown in Fig. 7, the representative photo-responsive $C$–$V$ profile of SIS devices with In/(Zn+In)=0.25 in the $a$-IZO layer gives $\Delta V$=0.13 V and, according to Eq. (1), $D_{it}=3.05\times10^{11}$ $cm^{-2}$ $eV^{-1}$ for such a sample is obtained. Similar measurements on SIS devices with In/(Zn+In)=0.4 and In/(Zn+In)=0.5 in the $a$-IZO layer give $D_{it}=8.85\times10^{10}$ and $D_{it}=3.26\times10^{10}$ $cm^{-2}$ $eV^{-1}$, respectively. The suppression of $D_{it}$ due to the increase of In/(Zn+In) ratio can be readily seen. Note that the SIS sample in fact contains the $a$-IZO/$SiO_x$ and $SiO_x$/Si interfaces. It is inferred that the variation of $D_{it}$ delineated above should mainly correlate with the $a$-IZO/$SiO_x$ interface since the growth condition of $SiO_x$ layer on Si substrate is fixed in this study. The properties of $SiO_x$/Si interfaces in all samples could thus be regarded as the same and their contribution to the change of $D_{it}$ could be neglected.

In order to clarify the roles of the bulk defects in $a$-IZO layer and that of the interfacial traps at $a$-IZO/$SiO_x$ interface, $C$–$V$ measurements were also performed on the Al/$a$-IZO/Al and Al/$a$-IZO/$SiO_x$ capacitor samples. Fig. 8(a) and (b) separately shows the $C$–$V$ profiles of the Al/$a$-IZO/Al MIM capacitor sample and $a$-IZO/$SiO_x$/Si MOS capacitor samples with the In/(Zn+In) ratios of 0.25 and 0.5. The insets in these figures show the device configurations and we note that the thickness of $SiO_x$ layer in $a$-IZO/$SiO_x$/Si MOS capacitor samples has been increased to about 40 nm in order to obtain appropriate capacitance data. Fig. 8(a) indicates that both samples exhibit very similar $C$–$V$ behaviors with relatively low capacitance densities, about 0.01 fF $\mu m^{-2}$ at an applied bias of 1 V, implying that the bulk defect density in the $a$-IZO layer is relatively insensitive to the In/(Zn+In) ratio. Thought the zinc vacancies in ZnO is escalated by the increase of $In_2O_3$ content *via* the defect reaction $In_2O_3 \xrightarrow{ZnO} 2In^{\bullet}_{Zn} + 3O_O + V''_{Zn}$, such an effect might be smeared out since the nano-crystalline IZO layer might be abound of the crystalline defects. Hence, the change of

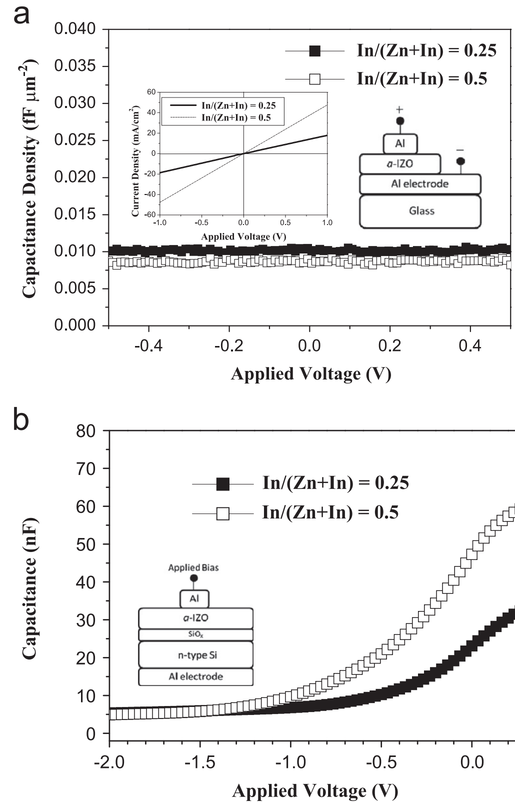


**Fig. 8.** (a) $C$–$V$ profiles of the Al/$a$-IZO/Al capacitor samples. The insets show the plot of the sample structure and the $J$–$V$ curves of samples with In/(Zn+In)=0.25 and 0.5. (b) $C$–$V$ characteristics of $a$-IZO/$SiO_x$/Si MOS capacitor samples obtained at 100 kHz and the inset shows the MOS sample structure.

In/(Zn+In) ratio affects the bulk defect density of $a$-IZO layer insignificantly.

Fig. 8(b) depicts a shaper transition of capacitance from the depletion region to the accumulation region for the MOS capacitor sample of In/(Zn+In)=0.5 in comparison with that for sample of In/(Zn+In)=0.25. This implies a well-formed $a$-IZO/$SiO_x$ interface in the sample of In/(Zn+In)=0.5 [23]. Moreover, the addition of $In_2O_3$ in ZnO has been demonstrated to promote the n-type conduction by increasing the number of free carriers (electrons) in ZnO. For sample of In/(Zn+In)=0.5, the larger electron concentration obtained in such an $a$-IZO layer (Fig. 2) may have, at least, partially alleviated the carrier trapping and hence reduced the effective $D_{it}$ at the $a$-IZO/$SiO_x$ interface. Consequently, increasing the In content of the $a$-IZO layer would benefit the $V_{oc}$ and short-circuit current density ($J_{sc}$) simultaneously and should play as the dominant factor in enhancing the performance of the SIS devices prepared in this study.

Fig. 9 presents the $J$–$V$ characteristics for the SIS devices measured under the AM1.5 illumination condition and the $V_{oc}$, $J_{sc}$, fill factor ($FF$) and $\eta$ deduced from these $J$–$V$ profiles are summarized in Table 1. It is evident from Table 1 that both $V_{oc}$ and $J_{sc}$ are increased with increasing the In/(Zn+In) ratio for these $a$-IZO/$SiO_x$/$n$-Si SIS solar cells. In particular, for the In/(Zn+In)=0.5 sample, a remarkable $\eta$ of 8.4% was obtained with the corresponding $V_{oc}$, $J_{sc}$ and $FF$ being of 0.38 V, 45.1 mA $cm^{-2}$ and 49.7%, respectively. Fig. 10 presents the IPCE profile for the SIS device with In/(Zn+In)=0.5. The IPCE values exceed 80% at the wavelength range of 400 to 900 nm, decrease with the increase of wavelength, and drop to about 10% when the wavelengths are greater than 1100 nm. This indicates the incident light is mainly absorbed by Si with $E_g$=1.1 eV (=1127 nm), that is, the charge carriers are generated by the irradiation of light with energy

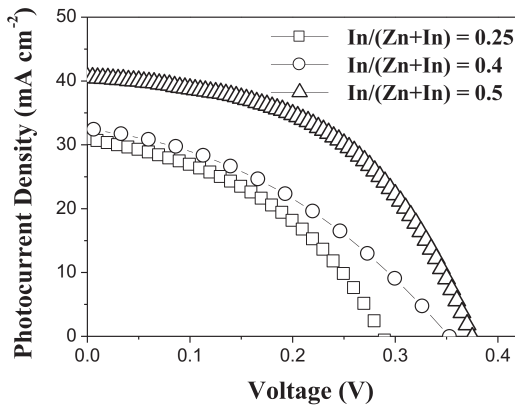


**Fig. 9.** $J$–$V$ characteristic of $a$-IZO/SiO$_x$/$n$-Si SIS devices measured at the AM1.5 illumination condition.

**Table 1**
Photovoltaic characteristics of SIS solar cells with different In contents.

| In/(Zn+In) (at%) | SiO$_x$ thickness (nm) | $V_{oc}$ (V) | $J_{sc}$ (mA cm$^{-2}$) | $FF$ (%) | $\eta$ (%) |
|---|---|---|---|---|---|
| 0.25 | 1.88 | 0.29 | 30.86 | 41.50 | 3.69 |
| 0.4 | 1.99 | 0.37 | 31.58 | 44.46 | 5.16 |
| 0.5 | 2.03 | 0.38 | 45.05 | 49.67 | 8.38 |

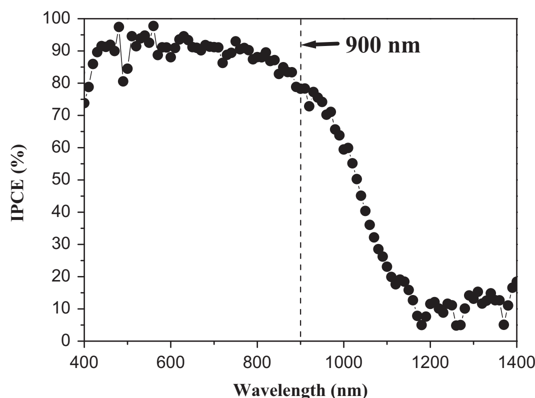


**Fig. 10.** IPCE profile for $a$-IZO/SiO$_x$/$n$-Si SIS devices prepared at In/(Zn+In)=0.5.

greater than 1.1 eV and transported from Si to TCO layer *via* the tunneling process [1,2].

Since in the present study the only tuning parameter was the In/(Zn+In) ratio used for preparing the $a$-IZO layer, it should be interesting to elaborate the possible underlying mechanisms in more details. For a solar cell, in general, the $\eta$ value is determined mainly by three factors: (i) extensive photon harvesting; (ii) efficient separation of photo-excited carriers and (iii) the swiftness of carrier passage to external electrodes. The first factor has to do with the properties of the light absorption layer (*i.e.*, the $n$-Si substrate in our case), which is relatively irrelevant to the present study. We have addressed the second factor in our previous studies and found that the SiO$_x$ thickness giving rise to the best performance of the $a$-IZO/SiO$_x$/$n$-Si SIS devices should be about 1.8 to 2.0 nm [6,7]. The thickness of this insulating layer was optimized to obtain a balance between the built-in field and the tunneling efficiency to drive the photo-excited carriers from the $n$-Si substrate to the $a$-IZO layer. Again, in the present study, we had fixed the condition of growing this layer in the PLD chamber under exactly the same condition. Thus, it should not be the primary reason for the observed differences. For the third factor, one would like to have smaller numbers carrier trap sites in both the bulk of the $a$-IZO layer and at the $a$-IZO/SiO$_x$ interface (to prevent the photo-excited carriers from being trapped along their journey to the electrodes) as well as larger carrier mobility in the $a$-IZO layer (to allow the photo-excited carriers to move toward the electrode once they tunnel through the SiO$_x$ insulating layer). Within the context of this scenario, one should be able to further improve the performance of SIS devices by reducing $D_{it}$. In fact, the increase in $V_{oc}$ and $J_{sc}$ obtained by increasing the In/(Zn+In) ratio in the $a$-IZO layer described above can also be explained within the same context. First, the $C$–$V$ measurements shown in Figs. 7 and 8 clearly indicated that the increased In/(Zn+In) ratio in the $a$-IZO layer dramatically lowered the effective $D_{it}$ at $a$-IZO/SiO$_x$ interface, presumably due to charge compensation on the interface sites. This not only would lead to the increment of built-in electric field near the interface and change $\phi_B$, but also would reduce the recombination centers at $a$-IZO/SiO$_x$ interfaces to provide additional tunneling current and lower the series resistance ($R_s$) of the device, giving rise to an improvement in $J_{sc}$ as seen in $a$-IZO layer with high In/(Zn+In) ratio. Finally, the slightly increased carrier mobility with increasing In/(Zn+In) ratio (see Fig. 2) may also contribute to the overall enhancement of the performance of the present $a$-IZO/SiO$_x$/$n$-Si solar cells.

## 4. Conclusions

In summary, we demonstrated a simple process to fabricate $a$-IZO/SiO$_x$/$n$-Si solar cells by directly depositing $a$-IZO layers on the n-type Si substrates subjected to appropriate dry oxidation treatment. The ultra-thin SiO$_x$ layer formed on the Si surface during PLD deposition has been found to be crucial for the performance of the SIS devices in our previous studies. Present study further illustrates that the increase of the In content in $a$-IZO layer suppresses the effective $D_{it}$ and $R_s$ of the SIS devices, resulting in a substantial improvement of device performance. For the $a$-IZO layer with In/(Zn+In)=0.5 deposited at 250 °C, a corresponding SiO$_x$ layer about 2-nm thick and low $D_{it}$ value around $10^{10}$ cm$^{-2}$ eV$^{-1}$ were obtained. Moreover, the SIS device containing such $a$-IZO layer exhibited a $\eta$ value of 8.4% with the $V_{oc}$, $J_{sc}$ and $FF$ being of 0.38 V, 45.1 mA cm$^{-2}$ and 49.7%, respectively. Our results evidently point an efficient way of fabricating and improving the performance of SIS-type solar cells.

## Acknowledgment

This work is supported by the National Science Council, Taiwan, ROC, under the contracts No. NSC100-2221-E-009-055-MY3 and No. NSC101-2112-M-009-015-MY2. JYJ is supported in part by the MOE-ATU program operated at NCTU.

## References

[1] J. Shewchun, J. Dubow, A. Myszkowski, R. Singh, The operation of the semiconductor–insulator–semiconductor (SIS) solar cell: theory, J. Appl. Phys. 49 (1978) 855–864.
[2] J. Shewchun, D. Burk, R. Singh, M. Spitzer, J. Dubow, The semiconductor–insulator–semiconductor (indium tin oxide on silicon) solar cell: characteristics and loss mechanisms, J. Appl. Phys. 50 (1979) 6524–6533.
[3] M. Spitzer, J. Shewchun, D. Burk, The operation of the semiconductor–insulator–semiconductor solar cell: barrier height lowering through interface states, J. Appl. Phys. 51 (1980) 6399–6404.
[4] A.K. Ghosh, C. Fishman, T. Feng, SnO$_2$/Si solar cells-heterostructure or Schottky-barrier or MIS-type device, J. Appl. Phys. 49 (1978) 3490–3498.
[5] H. Kobayashi, H. Mori, T. Ishida, Y. Nakato, Zinc oxide/n-Si junction solar cells produced by spray-pyrolysis method, J. Appl. Phys. 77 (1995) 1301–1307.
[6] H.W. Fang, S.J. Liu, T.E. Hsieh, J.Y. Juang, J.H. Hsieh, Fabrication and characterization of amorphous In–Zn–O/SiO$_x$/n-Si heterojunction solar cells, Sol. Energy 85 (2011) 2589–2594.

[7] H.W. Fang, T.E. Hsieh, J.Y. Juang, Influences of $SiO_x$ layer thickness on the characteristics of In–Zn–O/$SiO_x$/$n$-Si Hetero-junction structure solar cells, Surf. Coat. Technol. 231 (2013) 214–218.
[8] J. Tan, M.K. Das, J.A. Cooper Jr., M.R. Melloch, Metal–oxide–semiconductor capacitors formed by oxidation of polycrystalline silicon on SiC, Appl. Phys. Lett. 70 (1997) 2280–2281.
[9] T. Hashizume, E. Alekseev, D. Pavlidis, K.S. Boutros, J. Redwing, Capacitance–voltage characterization of AlN/GaN metal–insulator–semiconductor structures grown on sapphire substrate by metalorganic chemical vapor deposition, J. Appl. Phys. 88 (2000) 1983–1986.
[10] M.P. Taylor, D.W. Readey, M.F.A.M. van Hest, C.W. Teplin, J.L. Alleman, M.S. Dabney, L.M. Gedvilas, B.M. Keyes, B. To, J.D. Perkins, D.S. Ginley, The remarkable thermal stability of amorphous In–Zn–O transparent conductors, Adv. Funct. Mater. 18 (2008) 3169–3178.
[11] N. Ito, Y. Sato, P.K. Song, A. Kaijio, K. Inoue, Y. Shigesato, Electrical and optical properties of amorphous indium zinc oxide films, Thin Solid Films 496 (2006) 99–103.
[12] T. Minami, T. Kakumu, S. Takata, Preparation of transparent and conductive $In_2O_3$–ZnO films by radio frequency magnetron sputtering, J. Vac. Sci. Technol., A 14 (1996) 1704–1708.
[13] N. Naghavi, A. Rougier, C. Marcel, C. Guery, J.B. Leriche, J.M. Tarascon, Characterization of indium zinc oxide thin films prepared by pulsed laser deposition using a $Zn_3In_3O_6$ target, Thin Solid Films 360 (2000) 233–240.
[14] C. Huang, M. Wang, Q. Liu, Y. Cao, Z. Deng, Z. Huang, Y. Liu, Q. Huang, W. Guo, Physical properties and growth kinetics of co-sputtered indium–zinc oxide films, Semicond. Sci. Technol. 24 (2009) 095019.
[15] H. Hosono, M. Yasukawa, H. Kawazoe, Novel oxide amorphous semiconductors: transparent conducting amorphous oxides, J. Non-Cryst. Solids 203 (1996) 334–344.
[16] D.S. Ginley, H. Hosono, D.C. Paine, Handbook of transparent conductors, in: H Hosono (Ed.), Transparent Amorphous Oxide Semiconductors for Flexible Electronics, Springer, New York, 2010, pp. 459–487.
[17] J.W. Jeon, D.W. Jeon, T. Sahoo, M. Kim, J.H. Baek, J.L. Hoffman, N.S. Kim, I.H. Lee, Effect of annealing temperature on optical band-gap of amorphous indium zinc oxide film, J. Alloys Compd. 509 (2011) 10062–10065.
[18] T. Moriga, Y. Hayashi, K. Kondo, Y. Nishimura, K. Murai, I. Nakabayashi, H. Fukumoto, K. Tominaga, Transparent conducting amorphous Zn–Sn–O films deposited by simultaneous dc sputtering, J. Vac. Sci. Technol., A 22 (2004) 1705–1710.
[19] A.J. Leenheer, J.D. Perkins, M.F.A.M. van Hest, J.J. Berry, R.P. O'Hayre, D. S. Ginley, General mobility and carrier concentration relationship in transparent amorphous indium zinc oxide films, Phys. Rev. B: Condens. Matter 77 (2008) 115215.
[20] J. Tauc, R. Grigorovici, A. Vancu, Optical properties and electronic structure of amorphous germanium, Phys. Status Solidi A 15 (1966) 627–637.
[21] K. Ramamoorthy, M. Jayachandran, K. Sankaranarayanan, P. Misra, L.M. Kukreja, C. Sanjeeviraja, Epi-$n$-IZO thin films/(1 0 0) Si, GaAs and InP by L-MBE-a novel feasibility study for SIS type solar cells, Sol. Energy 77 (2004) 193–201.
[22] J.P. Ponpon, P. Siffert, Open-circuit voltage of MIS silicon solar cells, J. Appl. Phys. 47 (1976) 3248–3251.
[23] H. Wang, Y. Wang, J. Zhang, C. Ye, H.B. Wang, J. Feng, B.Y. Wang, Q. Li, Y. Jiang, Interface control and leakage current conduction mechanism in $HfO_2$ film prepared by pulsed laser deposition, Appl. Phys. Lett. 93 (2008) 202904.